SAR Compliance Report for a Two-Coil Magnetic Charger

Model: A2458

FCC ID: BCGA2458

Date of Simulation:
06/01/2020-09/15/2020
Location:
Apple Inc., Cupertino, CA, USA

Table of Contents

1 Introduction

This report demonstrates RF exposure compliance, using SAR simulation, for WPT (Wireless Power Transfer) devices operating at 360 kHz and 326.5 kHz.
This product has two WPT transmitters (one for the phone and one for the watch) which are installed in a small charging pod ("puck") with magnets to secure the puck to the client. The charging session only occurs with the host (puck) connected to an AC power outlet. However, due to the puck being held in place by magnets, it is expected that customers may use the charging function in portable use conditions; charging the phone while making a call, or texting. All possible use cases for the two-coil WPT device, are summarized in a table -1, below.

Table -1

	Device	Frequency (kHz)	Certification Method
	New iPhone	360	SAR Simulation
	Apple watch & Legacy Apple watch	326.5	MPE Measurements
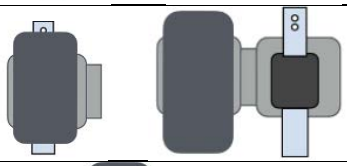	New iPhone, Apple watch & Legacy Apple watch	360 & 326.5	MPE Measurements
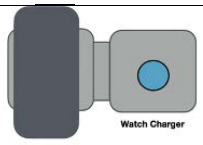	New iPhone	360	MPE Measurements
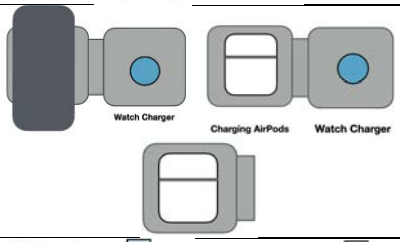	Legacy iPhone, Air pods	127	MPE Measurements
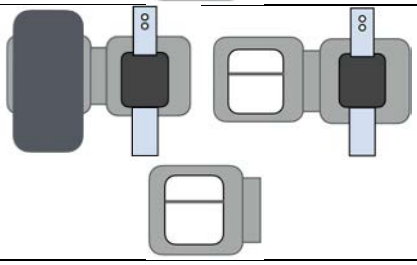	Legacy iPhone, Air pods, Apple watch & Legacy Apple watch	127 & 326.5	MPE Measurements

Among all of the use cases, only the first one in the table, is evaluated by simulation and the rest will be evaluated using measurement. Since at the operating frequency, the near-field H field strength may exceed the 1.63 A/m limit defined in §1.1310. Therefore, as permitted by §2.1093(d)(3) and Paragraph 3.d) of KDB 680106 D01, we use SAR numerical modeling to demonstrate compliance to the 1.6 W/kg localized 1-g SAR limit, due to the unavailability of SAR measurement tools and procedures.

Applying the SAR limit is also justified because:

1. The §1.1310 limits are intended for mobile whole-body exposure condition and are therefore far too stringent for local exposure conditions. In contrast, the §2.1093 local exposure limit is 20 times the whole-body SAR limit, and extremity exposure (held-in-hand) limit is 50 times higher.
2. The current H-filed limits specified in international standards (IEEE and ICNIRP) are much higher than 1.63 A/m at 360 kHz.

The following sections describe the modeling, measured H-field, simulated H-field, and simulated SAR for a charging pod and a handset client.

2 Wireless Power Transfer System

The phone wireless power transfer system consists of a transmitting coil with 11 turns and measures 7.5 uH nominally in free air. The receiver coil consists of 13 turns and measures 9.06 uH nominally in free air. Both coils are single layer and wound spirally. The watch wireless charger has 12 turns and measures 7.5 uH in free air, it is double layer and wound spirally.

3 SAR Simulations Methodology

The following steps have been taken to show the validity of the model used for SAR simulations:

1) EM Simulation:
    a. Import a CAD model that represents the actual product in the simulation tool.
    b. Define material properties inside the product based on vendor's inputs.
    c. Extract two-port network impedance matrix ([Z]) from the simulation.
2) Circuit Simulation:
    a. Include the impedance matrix in the wireless power transfer (WPT) circuit model.
    b. Run circuit simulation and extract coils' current waveforms.
3) Field, H-field, and SAR Calculations:
    a. Use the current waveforms to drive the EM simulation model.
    b. Calculate H-field from simulation.
    c. Compare simulated H-field with measured H-field.
    d. Once a correlation is established, this model will be used for SAR simulations.

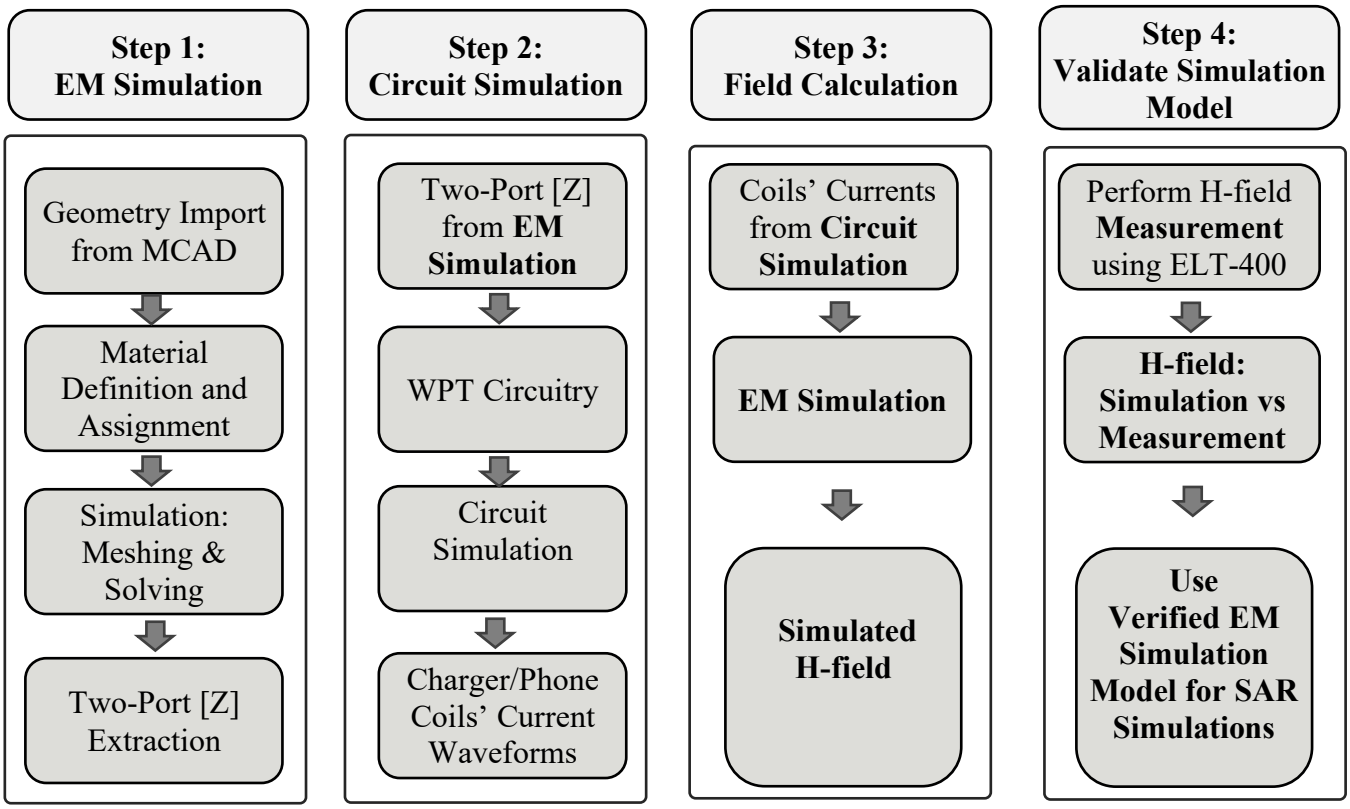

4 H-field Measurements

A Narda ELT-400 is used to measure the H-field above/below the DUT. A picture of the probe, an x-ray image of the probe, and the measurement setup are shown, below. The probe has three orthogonal loops with radius of 10mm. These loops are used to measure H-field in different directions.
The distance from the DUT to the probe is 0mm. However, the loops are covered with a plastic shell of 6mm thickness. Therefore, the distance from the center of the probe to the DUT is 16mm. These factors have been considered in simulation when calculating the H-field.

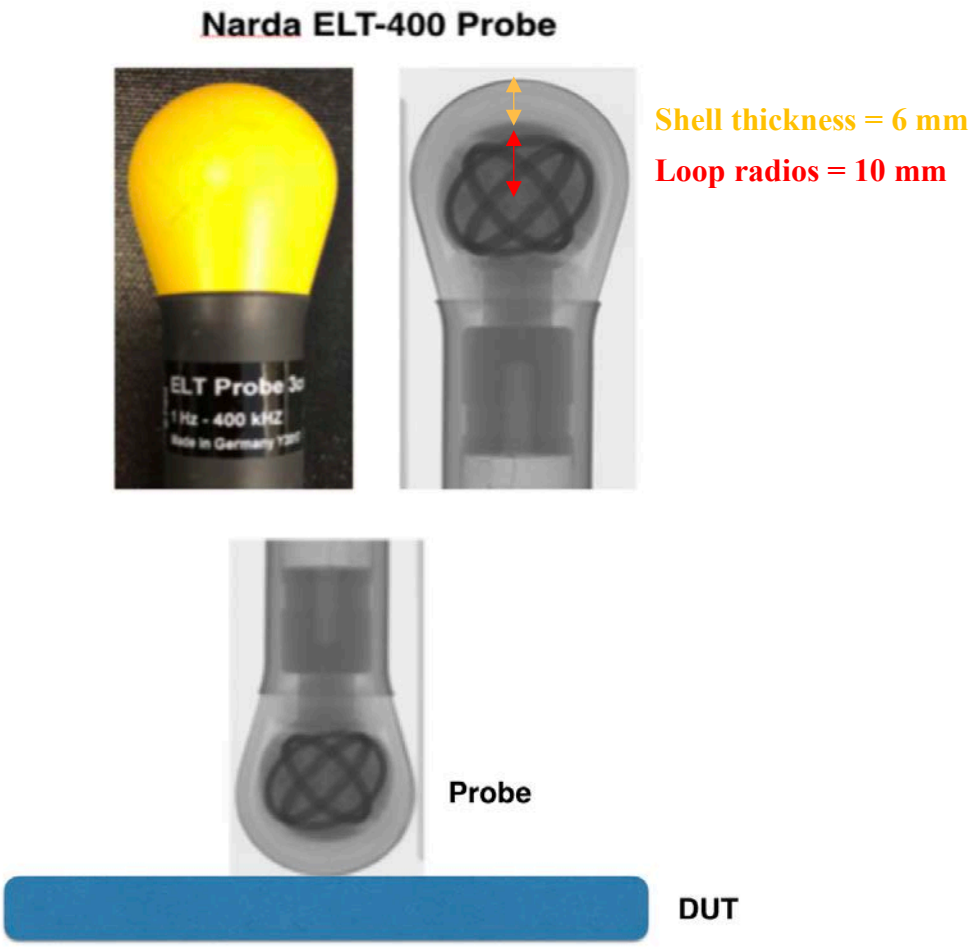

5 H-field Simulations

The electromagnetics simulations are conducted using commercially available software ANSYS HFSS. In order to validate the simulation model, H-field measurements are made on the DUT (as explained above) and compared to the simulated model results. The validated model is then used for the SAR simulations.

For the simulations, following Step 1 described above, the CAD file that represents the DUT is first imported. Then, the proper material properties are assigned at the operating frequency. After the simulation is completed, the two-port network [Z] was extracted and used with the WPT circuit model. This WPT model includes the charger source as well as the charging client side rectifier circuit. Solving the circuit using ANSYS Circuit tool, the proper excitation per transmitter (charger) and receiver (phone) coils are calculated. Later, these current waveforms are fed into the ANSYS HFSS to excite the coils and create H-field.

This wireless charger device can charge both phone and watch separately and/or simultaneously, as shown below. Also, it can operate in different configurations (i.e., flat or folded). Our investigations showed that the highest electromagnetic radiation and leakage potentially happens when the phone charger is charging the phone as it requires higher level of power compared to

the watch WPT. However, when the watch is not charging, it transmits a periodic pinging signal (frequency of 326.5 KHz, duty cycle of 14%) to search for the receiver (i.e., watch). We will evaluate the RF exposure to this pinging signal, as well.
Also, there are two main configurations for charging the phone as depicted in the figure, one is with the folded puck and the other one with the flat puck. When the charger set is in the flat configuration, it is extremely hard for user to hold the whole set with hand or place it on the body while the charger is working. So, this configuration does not qualify for on body application and it will be evaluated using measurement. However, with the folded configuration, there is a possibility that user carry the set close to the body while the charger is working. Hence, human body exposure is investigated for the folded configuration (a red dotted rectangle is added to distinguish this configuration from others).

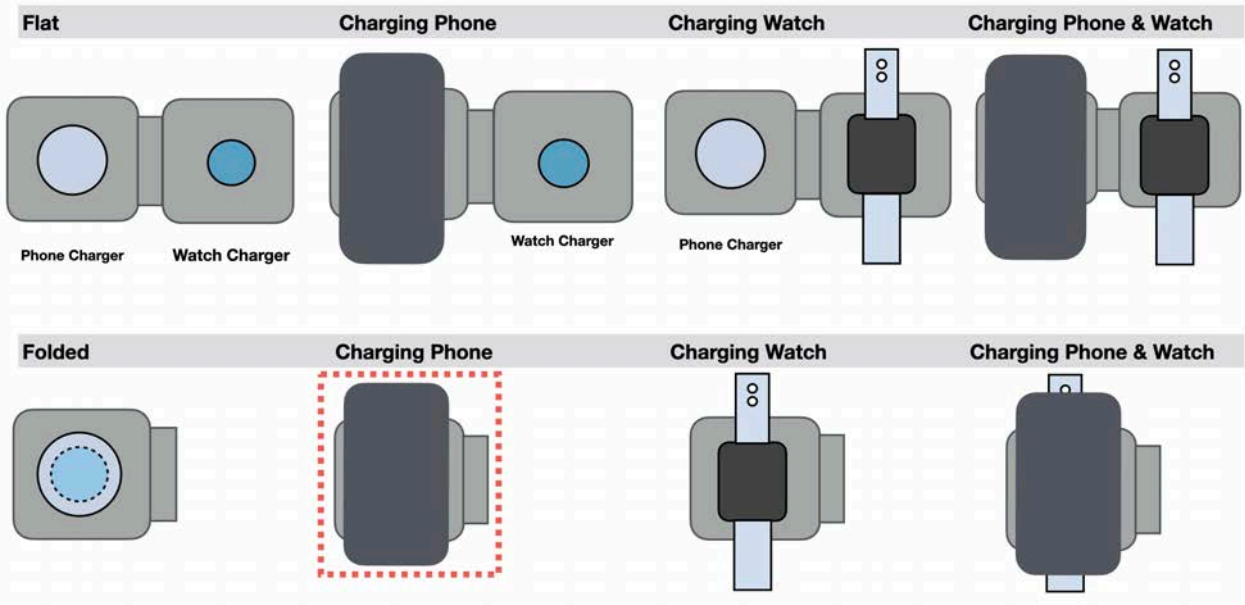

To make our study comprehensive, we included the misalignment and displacement. As shown below, the phone and the phone charger can be unintentionally forced by user to be laterally misaligned or vertically separated.

The only use case that was evaluated for SAR simulations is when Charger is folded and charging phone only, as this was the only realistic use case where the product is not bulky and can be held during operation, which qualifies it for on-body use case. Other use cases are not realistic because:
- If phone and watch are charging at the same time, product is bulky and can't be held
- AirPods and legacy phones doesn't have magnets and won't hold during portable case
- In Watch stand-alone case, there is no use case for anybody to hold the charger and use watch during charging.

All other use cases were evaluated with measurements as shown in the table -1.

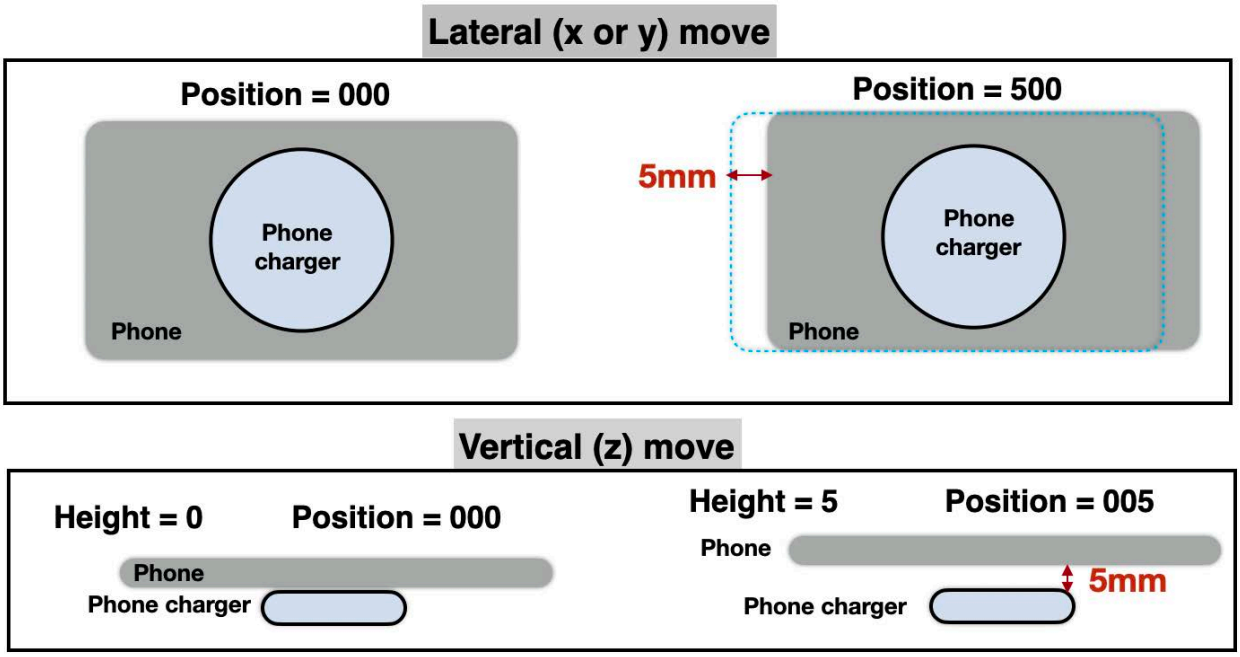

The misalignment and/or separation can change H-field's intensity and spatial distribution. Hence, several different misalignment and separation cases were selected and investigated to determine the worst-case scenario (i.e., highest H-field).
After simulating these cases, some will be selected and measured and used to benchmark the accuracy of the simulation model. Finally, a few cases will be selected for SAR and E-field simulation.

To this end, the simulation results are compared for the phone side, below. We should clarify that for the phone side, the H-field is dominated by the vphone charger and for the puck side, the H-field is dominated by the watch WPT's pinging signal that is used by the watch to detect presence of the watch.
For each side, the H-field probe is in contact with the DUT, scanning an area of 152 by 152 mm^2 with step size of 2 mm.

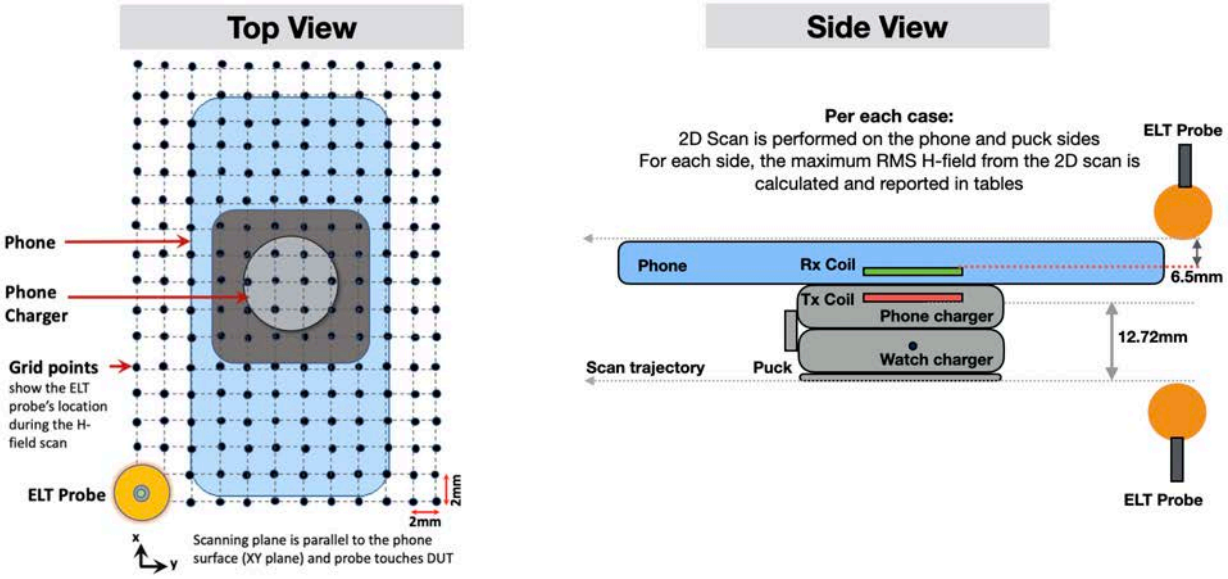

The maximum RMS H-field is reported in the tables (unit: A/m). The target power represents the maximum power that can be delivered to the phone for each case.

Phone Side RMS H-field (A/m), Folded Configuration

Phone's Relative Move (X,Y,Z) from Alignment	Target Power	Simulation	Measurement
(0,0,0)	15	1.07	0.50
(2,0,2)	15	1.66	0.96
(4,0,4)	7.5	1.74	0.98
(5,0,5)	3.5	1.76	0.76

Puck Side RMS H-field (A/m), Folded Configuration

Phone's Relative Move (X,Y,Z) from Alignment	Simulation	Measurement
(0,0,0)	7.6	5.40
(2,0,2)	7.6	5.38
(4,0,4)	7.6	5.39
(5,0,5)	7.6	5.31

To further evaluate the simulation model, we simulated and measured the puck only scenario (without the phone presence) and compared the H-field values when the probe moves at a vertical distance from front of the puck. The simulation and measurement curves are compared, below. There is a very good correlation between the measurement and simulation curves, verifying the accuracy of the model.

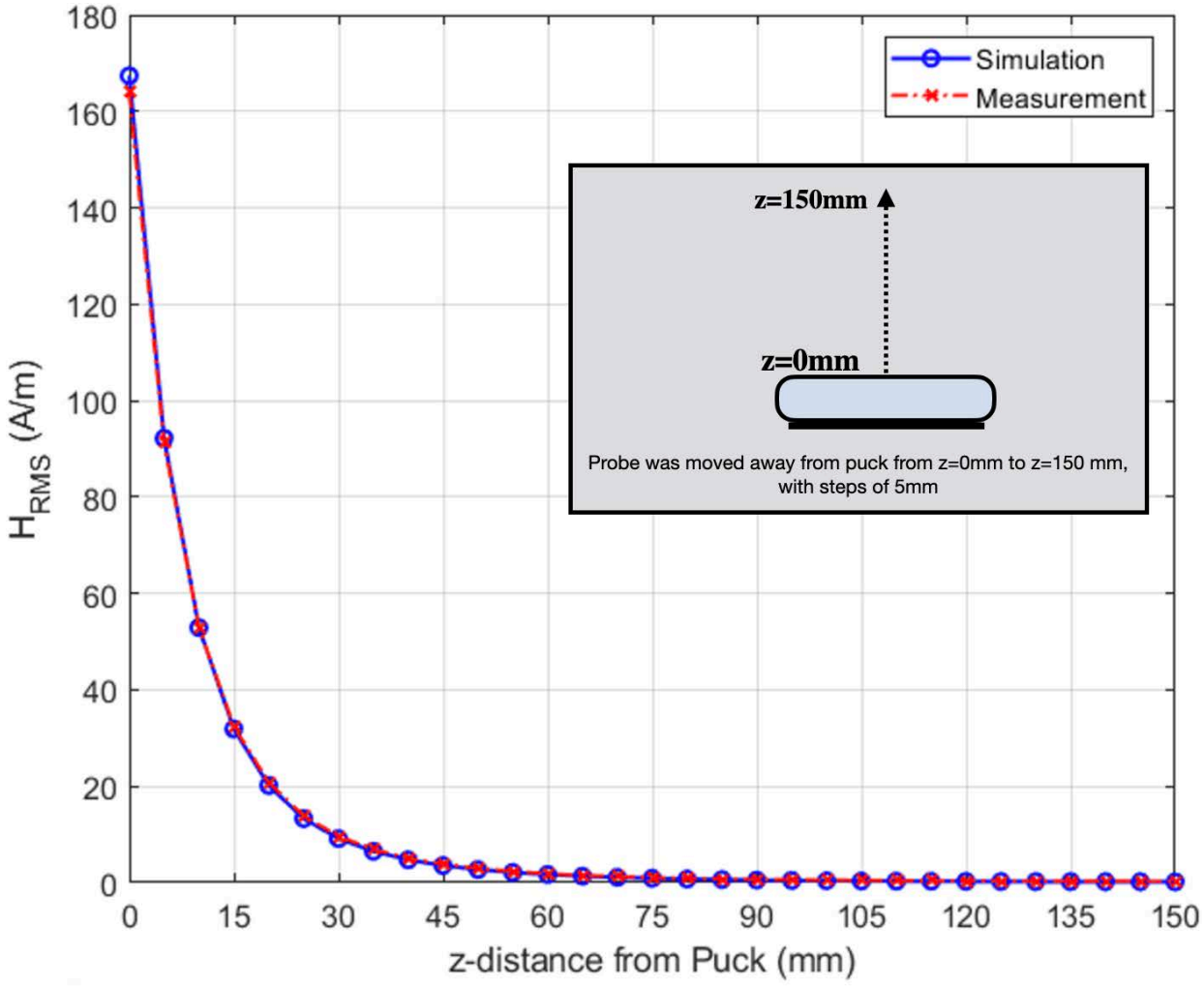

6 SAR Simulations

With correlation demonstrated between measurement and simulation, the same model is then used for SAR calculations with a phantom added in contact with the DUT. The simulations are computed on a 96 core CPU server with an available RAM of 4 Terabytes. For this simulation, the model run takes approximately 12 hours to complete.

The following steps are used for accurate SAR calculations:

1) Elliptical phantom used in body exposure measurements is commercially available from SPEAG: Outer Dimensions of 600mm x 400mm x 150mm.
2) Homogeneous tissue material is used as liquid for desired frequency.
3) Power loss in phantom is calculated.
4) Divide power loss by mass density to calculate SAR.

$$SAR = \frac{P_l}{\rho}$$

$$P_l = \text{Power loss density}$$

$$\rho = \text{Mass density}$$

5) Point SAR is averaged over 1g or 10g tissue.

Here, a mass density of 1000 Kg/m^3 is used for the modeling and the simulation of the phantom.

Human Tissue Material Properties at 360 kHz:
The worst-case scenario has been identified to be when a user is holding the device in hand and taking a call or holding the phone on their body while charging. The electrical properties for body and hand layers are shown below. Since the SAR phantom is homogenous, using the layers' properties, the worst-case scenario is selected and applied for the phantom properties. Therefore, for the SAR simulations, the phantom that has conductivity of 0.5 and permittivity of 5016 at the 360 kHz operating frequency is used.

Electrical Properties:
Based on our research this is what we recommend for εr and sigma (σ) values for body layers

Tissue	Thickness **(mm)**	Permittivity	Conductivity **(S/m)**
Skin	3	5016	0.16
Muscle	9	4666	0.5
Bone	20	1414	0.165
Worst case	100	5016	0.5

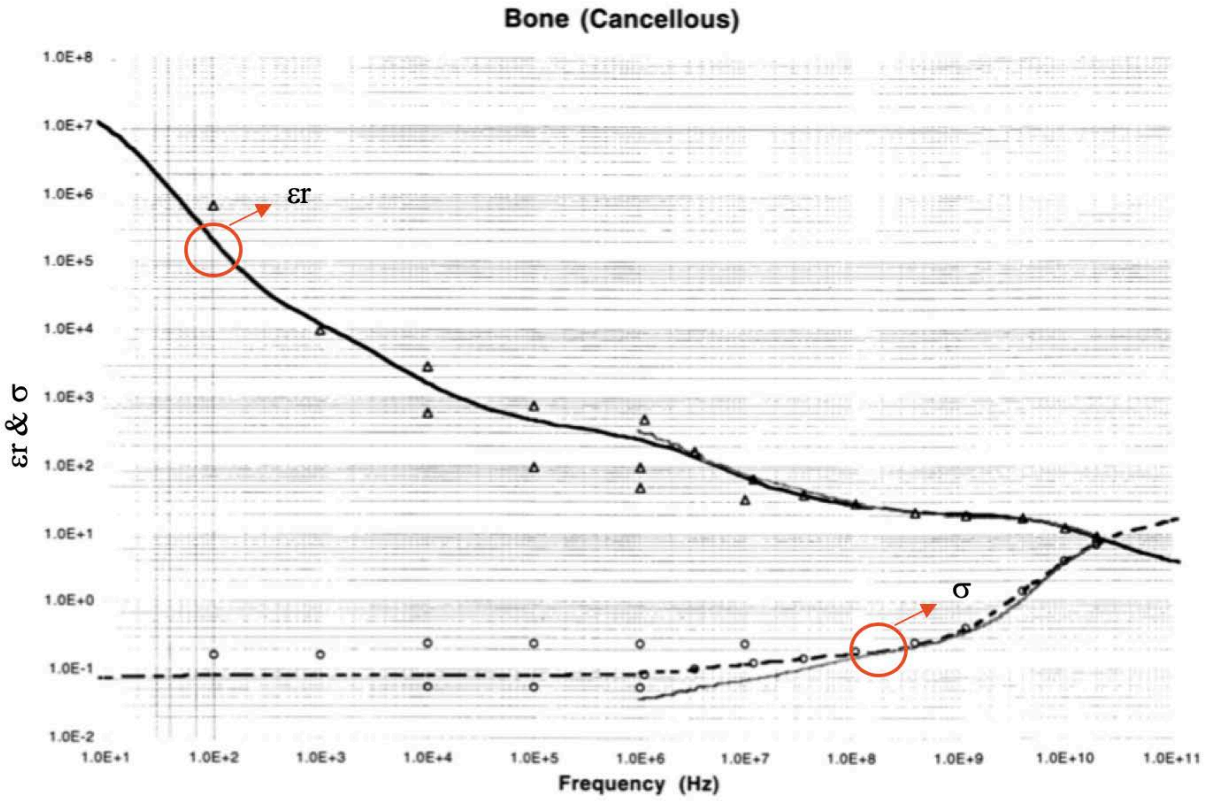
Bone (Cancellous)
εr & σ
1.0E+8
1.0E+7
1.0E+6
1.0E+5
1.0E+4
1.0E+3
1.0E+2
1.0E+1
1.0E+0
1.0E-1
1.0E-2
εr
σ
1.0E+1
1.0E+2
1.0E+3
1.0E+4
1.0E+5
1.0E+6
1.0E+7
1.0E+8
1.0E+9
1.0E+10
1.0E+11
Frequency (Hz)

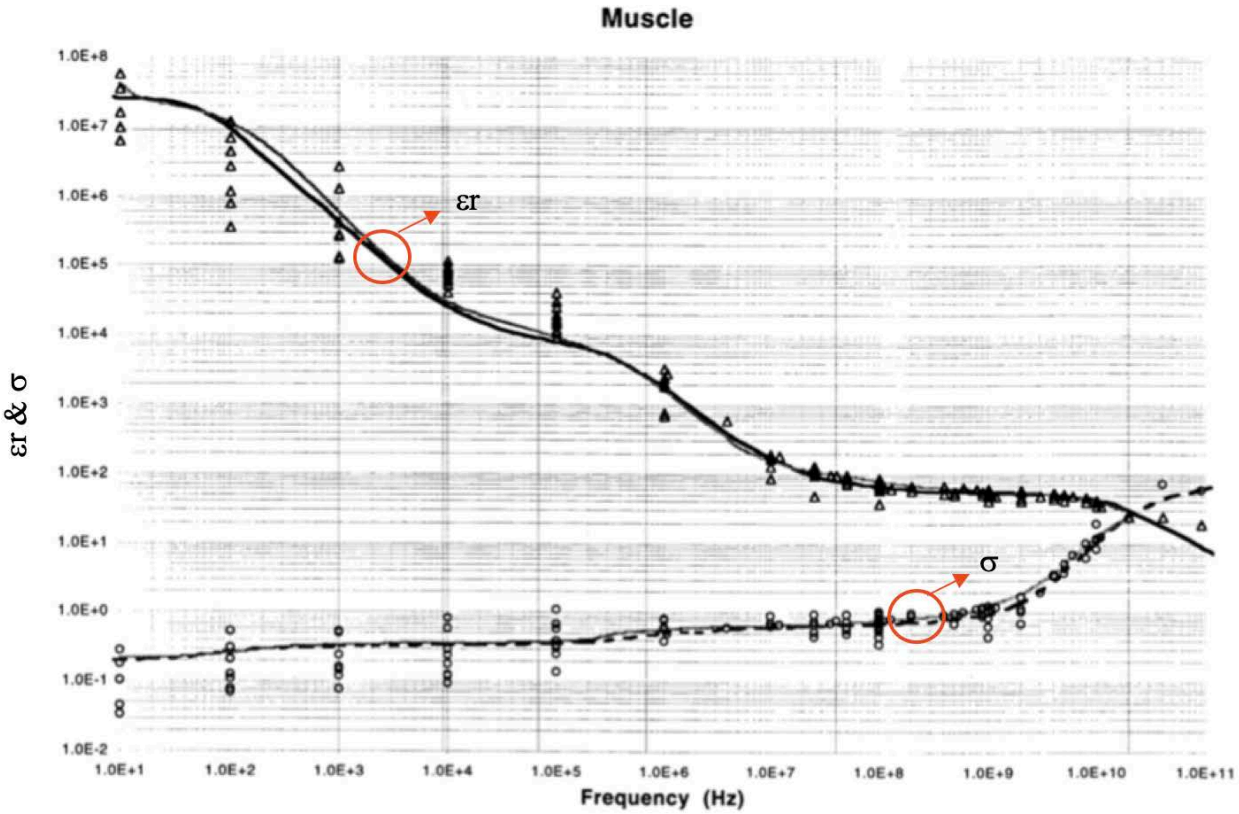
Muscle
εr & σ
1.0E+8
1.0E+7
1.0E+6
1.0E+5
1.0E+4
1.0E+3
1.0E+2
1.0E+1
1.0E+0
1.0E-1
1.0E-2
εr
σ
1.0E+1
1.0E+2
1.0E+3
1.0E+4
1.0E+5
1.0E+6
1.0E+7
1.0E+8
1.0E+9
1.0E+10
1.0E+11
Frequency (Hz)

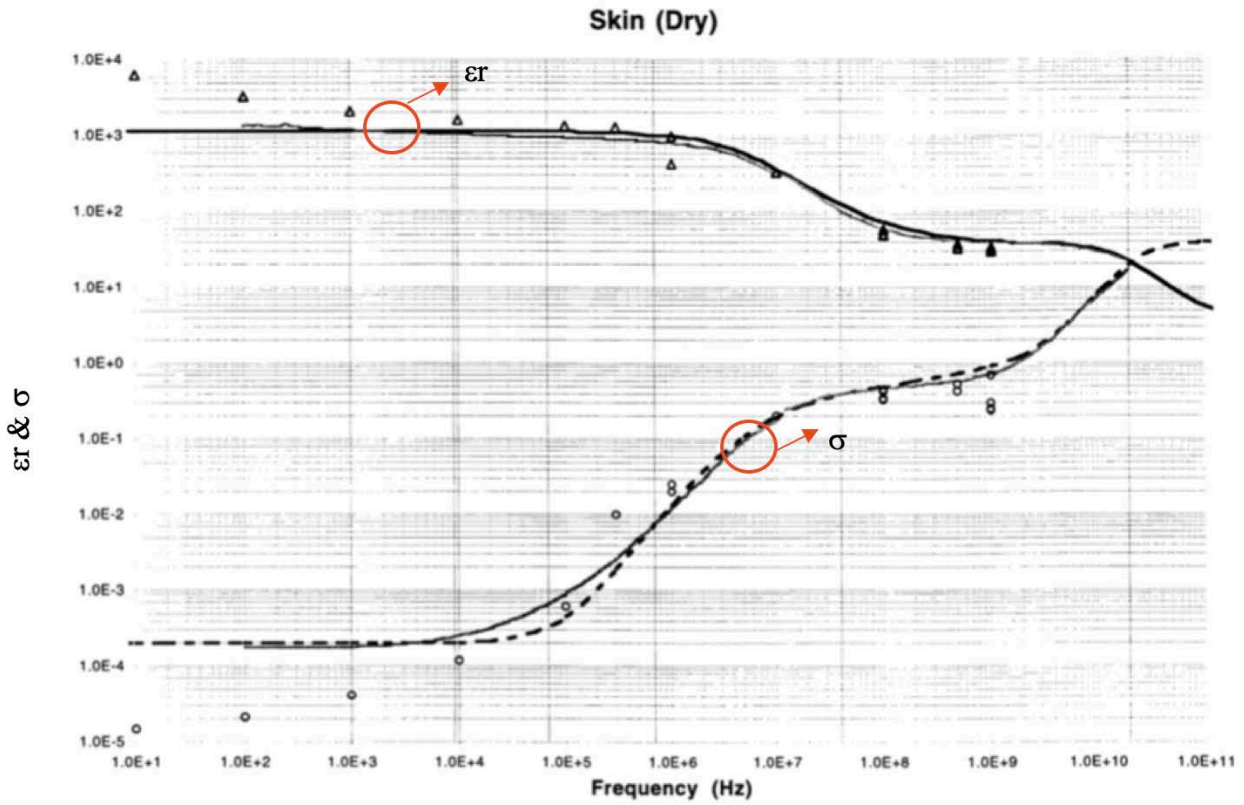

Mesh Adaptation:
HFSS adapts the mesh based on the field strength. It is important to ensure the mesh is refined to capture SAR accurately. This can be done by using adaptive meshing available in HFSS.

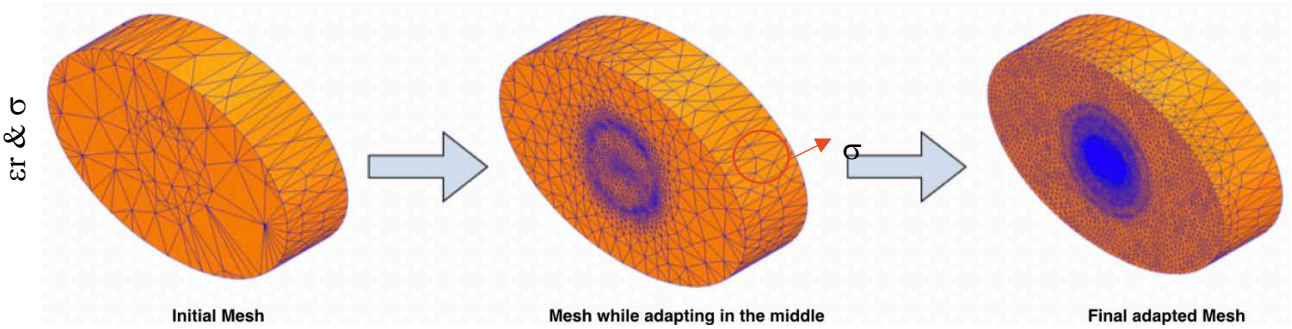

SAR Results:

Using the H-field simulation and measurement tables, two exposure cases were selected for SAR investigation. Considering that the phantom can be in contact with the phone or the back side of the folded puck (i.e., watch charger side), there is a total of four scenarios:

> **Exposure Case 000 (a):** Nominal configuration with perfect alignment and phantom placed above the receiver phone, hence exposed to phone charger leakage
> **Exposure Case 000(b):** Nominal configuration with perfect alignment and phantom placed below the puck, hence exposed to the watch charger leakage during the digital pinging
> **Exposure Case 505 (a):** Misaligned configuration with the worst-case alignment and phantom placed above the receiver phone, hence exposed to the phone charger leakage
> **Exposure Case 505 (b):** Misaligned configuration with the worst-case alignment and phantom placed below the puck, still dominated by leakage from the watch charger digital pinging.

In addition, two corner cases that are not likely to happen in normal application where the folded puck is in direct contact with the phantom and the charger is working with the highest current are investigated.

> **Direct Exposure Case 1(a):** with receiving phone unit absent and the phantom placed directly above the puck, exposed to the phone charger. The phone charger is excited with the highest current level among all of the charging cases (i.e., 2.7 A)
> **Direct Exposure Case 1(b):** with receiving watch unit absent and the phantom placed below the puck exposed to the watch charger. The watch charger is excited with the highest current level that it supports.

For all the exposure cases, dielectric properties (conductivity and permittivity) used for the phantoms are fixed as (permittivity: 5016, conductivity: 0.5). The coil properties are also fixed, phone charger transmitting coil with 11 turns and measures 7.5uH nominally in free air. The receiver phone coil consists of 13 turns and measures 9.06uH nominally in free air. Both coils are single layer and wound spirally. The watch charger coil has 12 turns, two layers, and wound spirally.
The following outputs are calculated and reported in the Table:

a. Peak spatial 1-g average SAR in tissue.
b. Peak spatially averaged electric field in tissue. Electric field is spatially averaged in a contiguous tissue volume of 2 mm x 2 mm x 2 mm.

The simulation results for the four exposure cases are shown, below. Please note that SAR and E field values for the cases where the phantom is in direct contact with the watch charger (i.e., both Case 000(b) and Case 505(b)) are reported for the watch charger pinging signal at 326.5 kHz since it dominates over the phone charger leakage. However, for the phone side exposure, the phone charger is dominant and hence, the results are reported for Case 000(a) and Case 505(a) are for the phone charger leakage at 360 kHz.

Folded Configuration

Exposure Case	Description	Peak Spatial Average SAR, W/Kg	Peak Spatial Avg E, V/m Averaged over 2x2x2 mm^3
Case 000 (a)	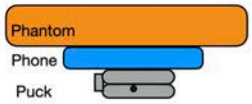	0.00000038	0.09
Case 000 (b)	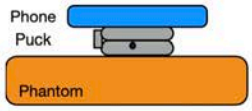	0.0062x0.14* = 0.000868	11.56**
Case 505 (a)	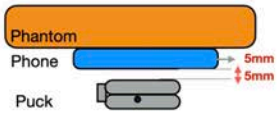	0.0000058	0.32
Case 505 (b)	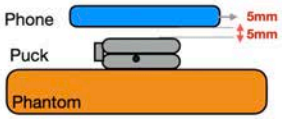	0.0062x0.14* = 0.000868	11.56**

* Watch pinging signal's duty cycle is 14%
**Peak E field is from the watch WPT's pining signal

Exposure Case	Description	Peak Spatial Average SAR, W/Kg	Peak Spatial Avg E, V/m Averaged over 2x2x2 mm^3
Direct Exposure (unrealistic) Case 1(a)		0.1081	34.5
Direct Exposure (unrealistic) Case 1(b)	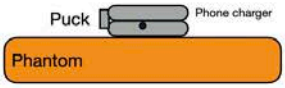	0.0109	15.27

The SAR plot is presented for Case000 (a). The peak spatial 1-g average SAR is 0.00000038 W/kg.

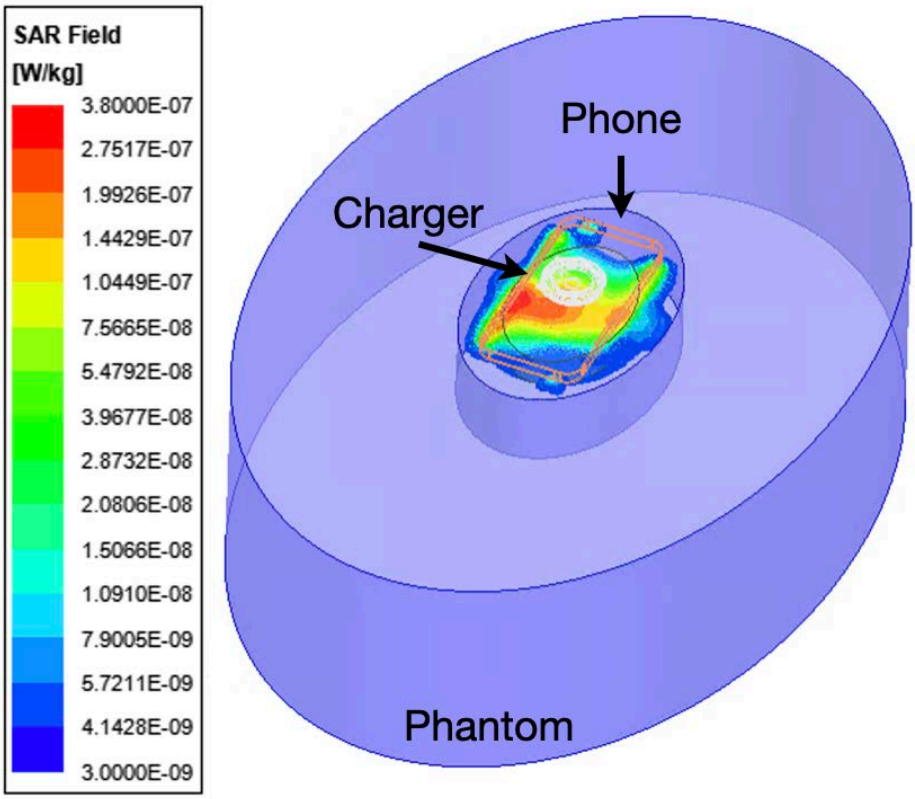

The side view is also presented, below.

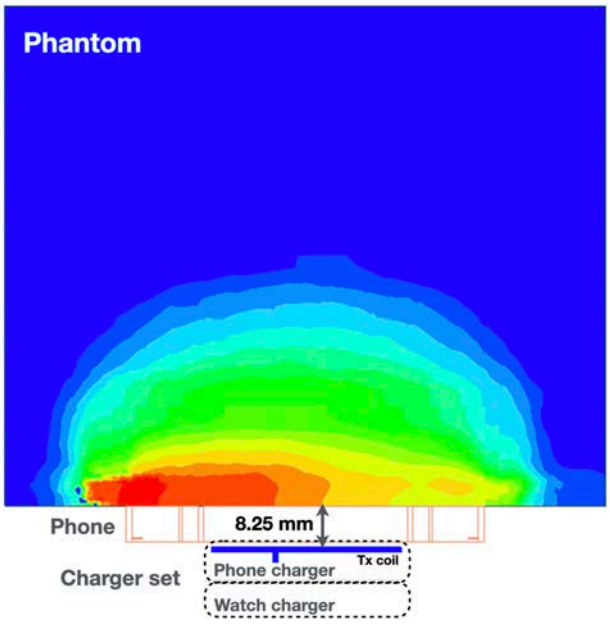

For the corner Case 1(a), the spatial average 1-g SAR is presented, below.

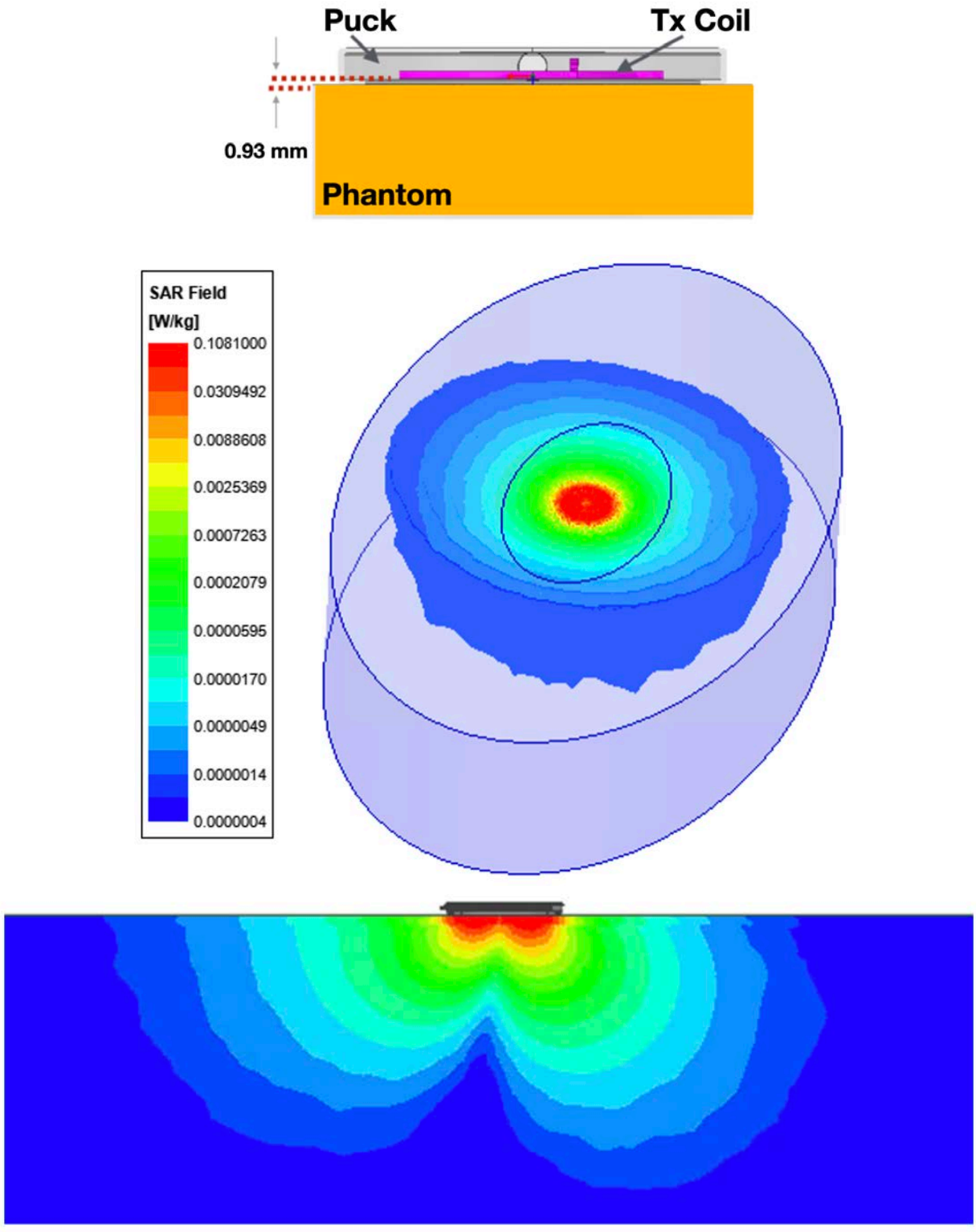

To show how the peak value would compare to the maximum allowable SAR limit, we manually changed the plotting scale and set the highest value to 1.6 W/Kg. As it can be seen below, the peak spatial SAR is much lower than the limit.

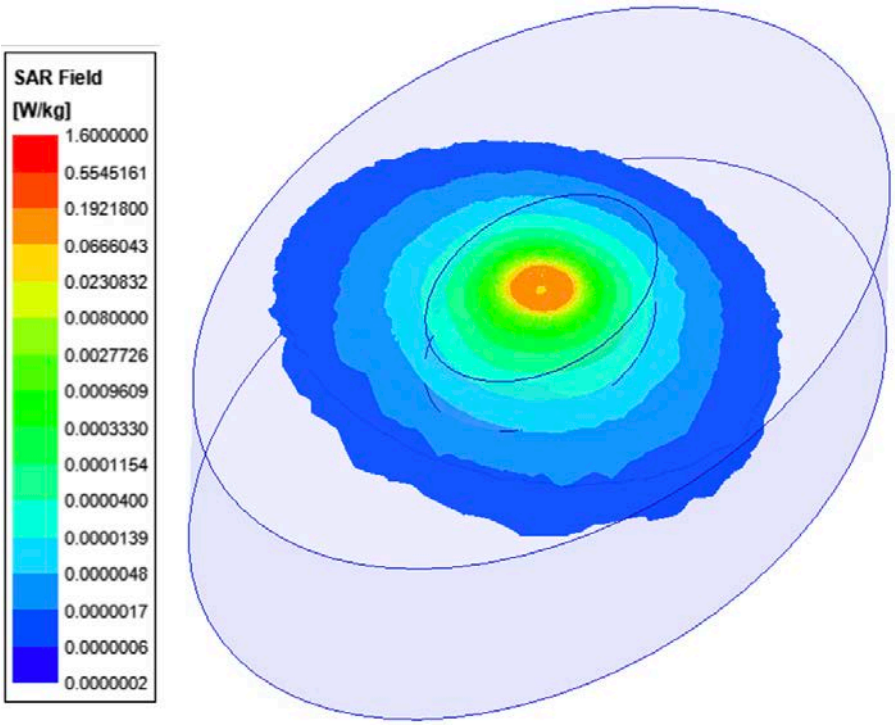

Note: The colormap scale is manually adjusted, the peak value of the spatial average SAR is only 0.1081 W/Kg.

Moreover, the E-field distribution inside the phantom for the Case1(a) is shown below. Please note that the value reported in the table above was averaged over a cube of 2mmx2mmx2mm and that explains why the value is lower than the peak E-field in this plot.

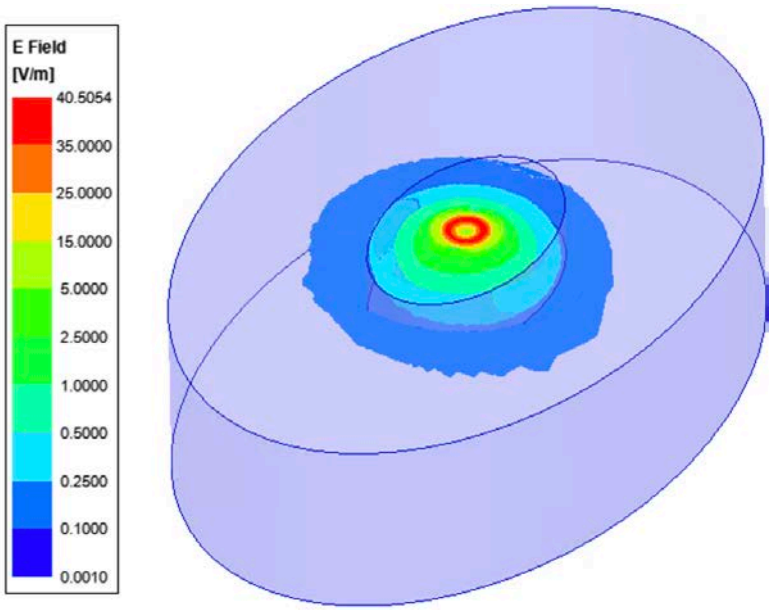

7 Summary

Based upon the above results, the accuracy of the SAR simulations is demonstrated by correlating H-field measurements to simulations. The validity of using this modeling and SAR computational method hence is established. For the nominal case where the puck and the phone are aligned without any vertical separation, the highest peak spatial 1-gram average SAR is 0.0000868 W/Kg and the highest peak spatial average E field (i.e., averaged over a cube of 2mmx2mmx2mm) is 11.56 V/m.

8 Annex A: specific information for SAR computational modelling

1) Computation Resources

The models were simulated on a 96 core CPU server with an available RAM of 4 Terabytes. Each model variation took around 12 hours to complete. Based on the simulation profile, the minimum resources needed to finish these simulations will be approximately 8 core CPU with 512GB of RAM. Using the minimum requirements simulation will likely take more time than 12 hours.

2) Algorithm implementing and validation

This section is divided into two parts. The code performance validation provides methods to determine that the finite-element algorithm in HFSS has been implemented correctly and works accurately within the constraints due to the finite numerical accuracy. It further determines the quality of absorbing boundary conditions and certain parts of the post processing algorithms that are part of HFSS. The second part has few canonical benchmarks. All benchmarks can be compared to analytical solutions of the physical problem or its numerical representation. The methods characterize the implementation of the finite-element algorithm used by HFSS in a very general way. They are defined such that it is not possible to tune the implementation for a particular benchmark or application without improving the overall quality of the code.

2.1) Code performance validation

2.1.1) Propagation homogeneous medium

A straight rectangular waveguide with ports on both ends is well suited as a first test of an implementation of the Finite-Element Method used by HFSS. The waveguide has a width of 20 mm, a height of 10 mm and a length of 300 mm. The waveguide is filled homogeneously with a material which, in three separate simulations, shall assume the following properties:

i. $\varepsilon r = 1, \sigma = 0 S/m$;
ii. $\varepsilon r = 2, \sigma = 0 S/m$;
iii. $Re(\varepsilon r) = 2$, $\sigma = 0.2 S/m$.

To verify that the mesh used by HFSS is independent of orientation, the waveguide has been rotated so that it is not parallel with any principal coordinate plane (XY, XZ, YZ). The waveguide is driven in the TE10 mode at 10 GHz. Reported are the magnitudes of S21 and S11, as well as the values of the real and imaginary parts of the propagation constant γ. The table 1, below provides the reference values [B1], acceptable result criteria, as well as the simulated results.

Table 1: Criteria for the waveguide evaluation

Re(ε_r)	1	2	2
σ	0	0	0.2
|S21| reference value	1	1	8.7 × 10-5
Criterion for |S21|	≥ 0.9999	≥ 0.9999	± 5 × 10-6
|S21| simulated results	1	1	8.7 × 10-5
|S11| reference value	0	0	0
Criterion for |S11|	≤ 0.003	≤ 0.003	≤ 0.003
|S11| simulated results	0	0	0
Re(γ) reference value	0	0	31.17 m-1
Criterion for Re(γ)	± 0.1 m-1	± 0.1 m-1	± 2%
Re(γ) simulated results	0	0	31.17
Im(γ) reference value	138.75 m-1	251.35 m-1	253.28 m-1
Criterion for Im(γ)	± 2%	± 2%	± 2%
Im(γ) simulated results	138.75	251.35	253.28

As is seen in the above table, HFSS easily meets the criteria for properly and accurately calculating the waveguide problem.

2.2.2) Planar dielectric boundary

In order to test the reflection of a plane wave by a dielectric boundary, a rectangular waveguide can again be used. It is well known that the TE10 mode can be thought of as a superposition of two plane waves [B1]. Each wave's direction of propagation makes an angle θ with the axis of the wave guide, given by

$$\cos^2\theta = 1 - (c/2af)^2 \quad (1)$$

where c is the speed of light, a is the width of the wave guide and f is the frequency. Assuming the axis of the waveguide is the Z axis and assuming the waveguide is filled with vacuum for Z>0 and filled with dielectric 1 with complex relative permittivity εr for Z<0, Fresnel reflection coefficients for the TE and the TM cases, defined as ratios of electric field strengths, are given by [B2]

$$R^{TE} = (k_{0,z} - k_{1,z}) / (k_{0,z} + k_{1,z}) \quad (2)$$

$$R^{TM} = (\varepsilon_r k_{0,z} - k_{1,z}) / (\varepsilon_r k_{0,z} + k_{1,z}) \quad (3)$$

where $k_{0,z}$ and $k_{1,z}$ denote the z component of the propagation vector of the plane wave in vacuum and in the dielectric, respectively. They can be evaluated through

$$k_{0,z} = k_0 \cos\theta \quad (4)$$
$$k_{1,z} = k_0 \sqrt{(\varepsilon_r - \sin^2\theta)} \quad (5)$$

Finally, ε_r is complex and is given by

$$\varepsilon_r = \mathrm{Re}(\varepsilon_r) - j\sigma/(2\pi f \varepsilon_0) \quad (6)$$

where $\mathrm{Re}(\varepsilon_r)$ denotes the real part of the relative permittivity and σ is the conductivity of the medium.
For this test, a 20 mm × 10 mm waveguide with a length of 60 mm, as shown in Figure 1, was created. The top half was filled with vacuum and the bottom half with dielectric.

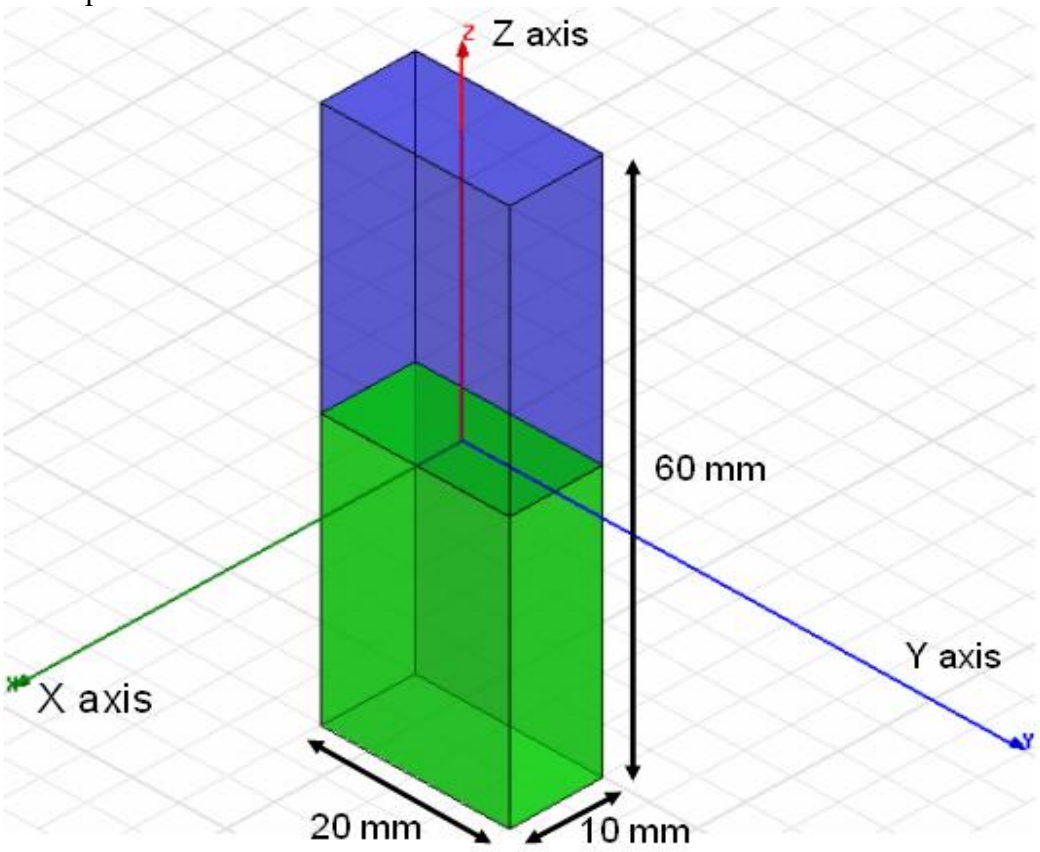

Figure 1: Waveguide filled half with vacuum and half with dielectric

In one copy of the model, all side walls were lossless metal, such that the dominant mode is the TE_{10} mode with propagation constant 138.75 m-1 at 10 GHz and represents the TE case in the reflection analysis. In the other copy of the model, the side walls that are parallel to the YZ plane were perfect magnetic conductors while the other walls were perfect electric conductors, such that the second mode (after a TEM mode which won't be used in this test) has propagation constant 138.75 m-1 at 10 GHz and represents the TM case in the reflection analysis.

Before simulation, the waveguides were rotated over an arbitrary angle such that no face is parallel with any coordinate plane. The waveguides were driven at 10 GHz in the proper mode.

In doing so, it is good practice to calculate all propagating modes, but the coupling between modes is expected to be negligible. Simulations were run for the cases of lossless and lossy dielectric as shown in Table 2. For the HFSS to pass the test, according to IEC 62704-1, the results need to be within 2% of the analytical values given in Table 2.

Table 2: Reflection at a dielectric interface

Re(εr)	σ (S/m)	RTE	RTE- Simulated	RTM	RTM - Simulated
4	0	0.4739	0.4739	0.1763	0.1763
4	0.2	0.4755	0.4755	0.1779	0.1779
4	1	0.5105	0.5105	0.2121	0.2121

As can be seen in table 2, HFSS produces results that are identical to the analytical results.

2.2) Canonical Benchmarks

The results for few low frequency benchmarks are summarized below. These benchmarks were used to validate the accuracy of the tool at low frequencies:

2.2.1) Dipole Antenna:

The following parameter were used in the dipole antenna to resonate at 400KHz.
Dipole length: 375 meters
Feed gap: 2.5 meters
Dipole Diameter: 5 meters

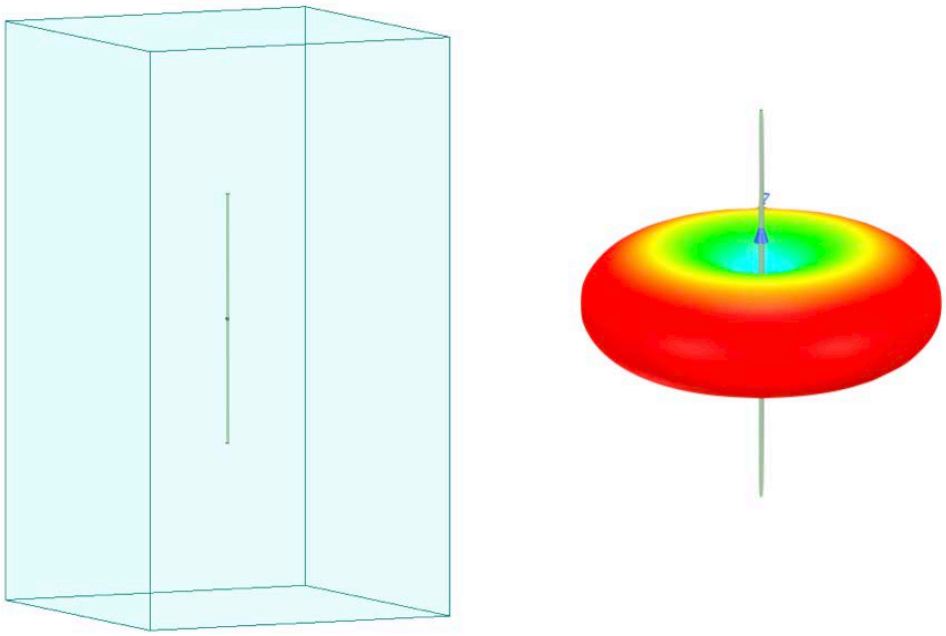

Figure 2: Dipole Antenna Model

The document IEC 62704-4 ED1 was referenced to compare the tables. Two computation methods were demonstrated as shown below to show the validity of the model.

Table 3: Simulated Dipole parameters

FEM Solver

Quantity	Simulation results	Tolerance	Satisfied?
Re(Z) at 400 KHz	**94.09**		
Im(Z) at 400 KHz	**55.62**		
Re(Z) at 320 KHz	**39.26**	$25\Omega < Re(Z) < 50\Omega$	Yes
Im(Z) at 320 KHz	**-90.52**	$-50\Omega < Im(Z) < -100\Omega$	Yes
Re(Z) at 360 KHz	**59.58**	$50\Omega < Re(Z) < 75\Omega$	Yes
Im(Z) at 360 KHz	**-18.30**	$-25\Omega < Im(Z) < 0\Omega$	Yes
Frequency for Im(Z) =0	**370**	$360MHz < f < 380MHz$	Yes
Maximum power budget error	**0.3**	$< 5\,\%$	Yes

MoM Solver

Quantity	Simulation results	Tolerance	Satisfied?
Re(Z) at 400 KHz	**98.45**		
Im(Z) at 400 KHz	**53.57**		
Re(Z) at 320 KHz	**43.31**	$25\Omega < Re(Z) < 50\Omega$	Yes
Im(Z) at 320 KHz	**-90.55**	$-50\Omega < Im(Z) < -100\Omega$	Yes
Re(Z) at 360 KHz	**65.03**	$50\Omega < Re(Z) < 75\Omega$	Yes
Im(Z) at 360 KHz	**-18.59**	$-25\Omega < Im(Z) < 0\Omega$	Yes
Frequency for Im(Z) =0	**370**	$360MHz < f < 380MHz$	Yes
Maximum power budget error	**0.02**	$< 5\,\%$	Yes

2.2.2) Toroid Inductor:

The parameters of the toroid were chosen to be
N = 20
A = 6.35e-4 m^2
R = 0.0263 m
ur = 64

The formula below gave an inductance of 139uH. The model created in HFSS gave an inductance of 139.9uH.

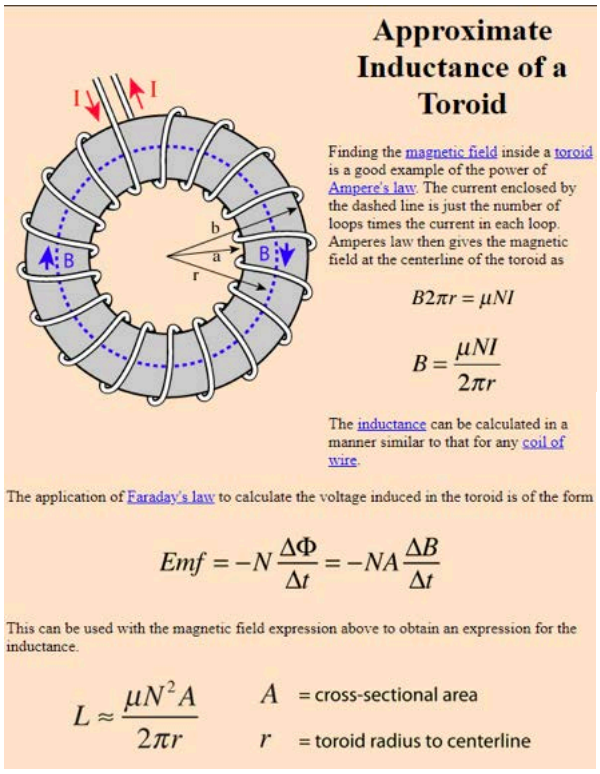

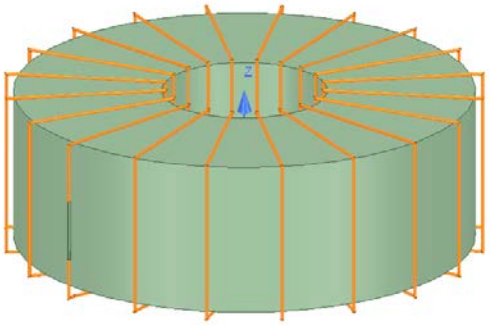

Figure 3: Toroid Model

2.2.3) Circular coil parallel to a flat, homogeneous phantom.:

The following benchmark is implemented using Equations 1-4 of the referenced Chen et al. (2014) paper and also matches Figure 6 therein scaled to 10 coil turns.

Below is the coil and phantom parameters:

Coil Diameter: 50 mm
Number of Turns: 10
RMS Current: 0.707 A (Peak current = 1 A)
Frequency: 100 kHz
Coil-to-Body Distance: 5 mm
Tissue Conductivity: 0.05 S/m
Tissue Permittivity: 1120

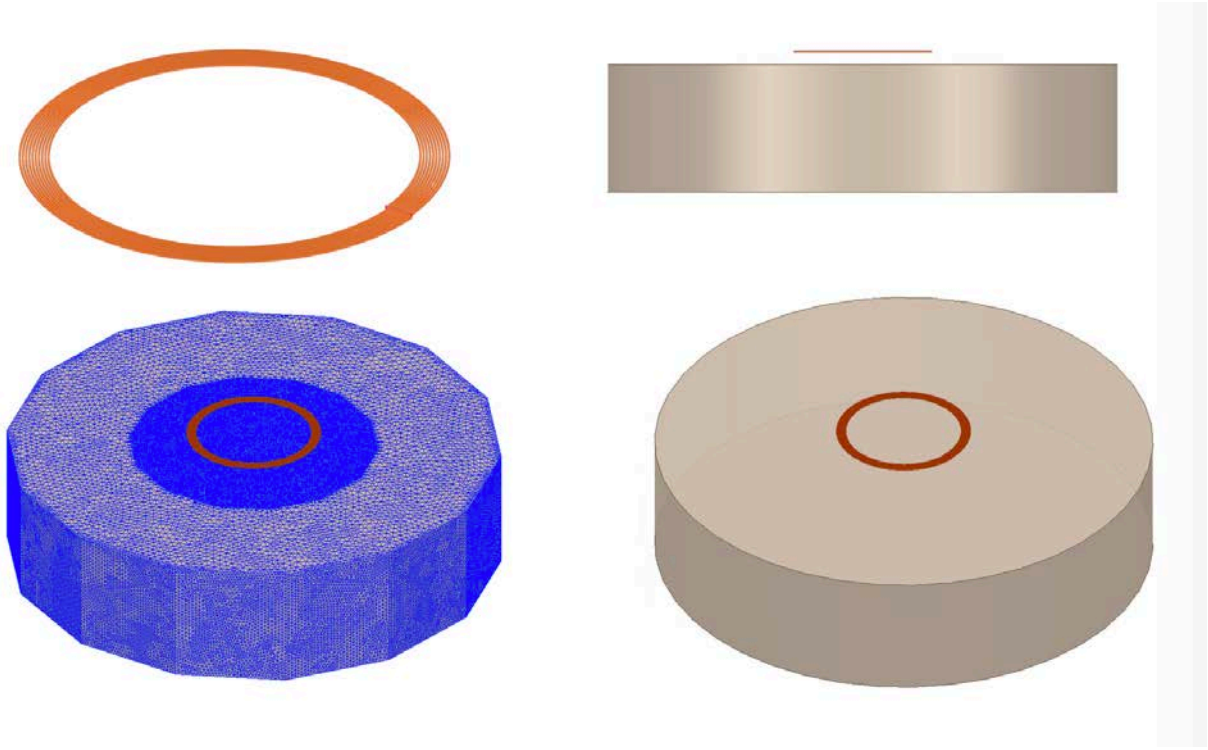

Figure 4: Current loop in front of a cuboid

The simulated spatial peak RMS electric field in tissue is 1.51 V/m compared to the analytical 1.47 V/m.

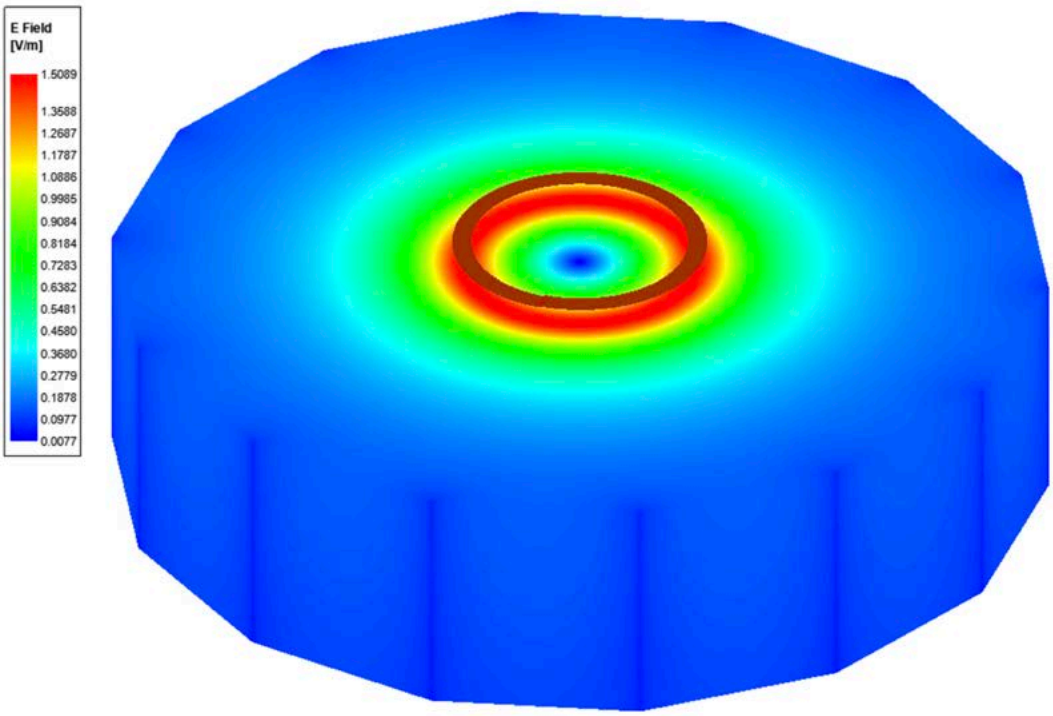

Figure 5: Current Density plot

3) Computational peak SAR from peak components & One-gram averaged SAR procedure

The calculation method for SAR follows IEEE P1528.4. Once the solver calculated the S-Parameter results, different coils can be driven and the result from the S-Parameter calculation is automatically scaled to the driving current of the coils. This result combination provides the correctly scaled power loss density in the phantom. The SAR calculation computes the local SAR first using electric field and conducting current:

$$SAR = \vec{E} \bullet \vec{J}_{conj}/(2\rho)$$

Afterwards the local SAR is averaged over a specific mass, usually 1g or 10g. As described in [IEEE P1528.4] the mass averaging is done by mapping the results to a structured hexahedral grid and afterwards the averaging scheme for FDTD per [IEEE P1528.4] is applied. The SAR calculation on the hexahedral grid is compliant with IEC 62704-1.

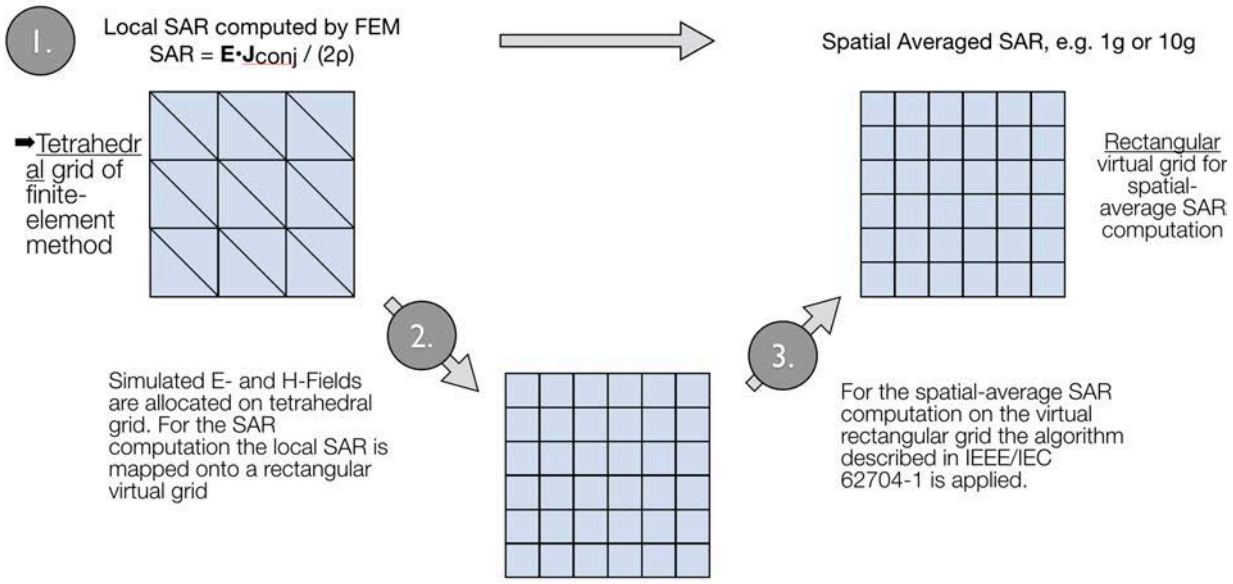

Figure 6: IEEE P1528.4 for SAR computation

4) Total Computational Uncertainty

Below is a table summarizing the budget of the uncertainty contributions of the numerical algorithm and of the rendering of the simulation setup. The table was filled using the IEC 62704-4 ED1 from 2018.
For the simulations, the direct exposure case where the phantom is placed directly in front of the puck is considered.

Table 6. Budget of uncertainty contributions of the numerical algorithm (filled based on IEC 62704-4 ED1).

a	b	d	e	g
Uncertainty component	**Subclause**	**Probability distribution**	**Divisor f(d, h)**	**Uncertainty %**
Mesh resolution	7.2.3	N	1	**0.01**
ABC	7.2.4	N	1	**0.08**
Power budget	7.2.5	N	1	**0.0**
Convergence	7.2.6	R	1,73	**0.01**
Phantom dielectrics	7.2.7	R	1,73	**0**
Combined standard uncertainty (k = 1)				**0.1**

Below is a table summarizing the budget of the uncertainty of the developed model. The table was filled using the IEC 62704-4 ED1 from 2018.

Table 7. Measurement uncertainty table.

a	b	d	e	g
Uncertainty component	**Subclause**	**Probability distribution**	**Divisor f(d, h)**	**Uncertainty %**
Uncertainty of the DUT model (based on near field distribution)	7.2.2	N	1	**2.12**
Uncertainty of the measurement equipment and procedure	7.2.3	N	1	**4**
Combined standard uncertainty (k = 1)				**6.12**

SAR calculations are also performed using specific standard anthropomorphic model (SAM) for the use-case of the WPT device described in this report. The use-case for the WPT device is shown in below. SAM accurate model with appropriate frequency-dependent SAM tissue dielectric properties are used in the simulation [Ref. 3]. The average SAR is calculated for the worst-case scenario with peak current of 3A as the input excitation source for the coil. The average SAR value is 0.0057 W/Kg. The SAR values from anatomical model is much lower than worst case scenario used in the main section, which only impacts the uncertainty calculation in the negative direction, making the presented data in section 6 always representing worst case numbers.

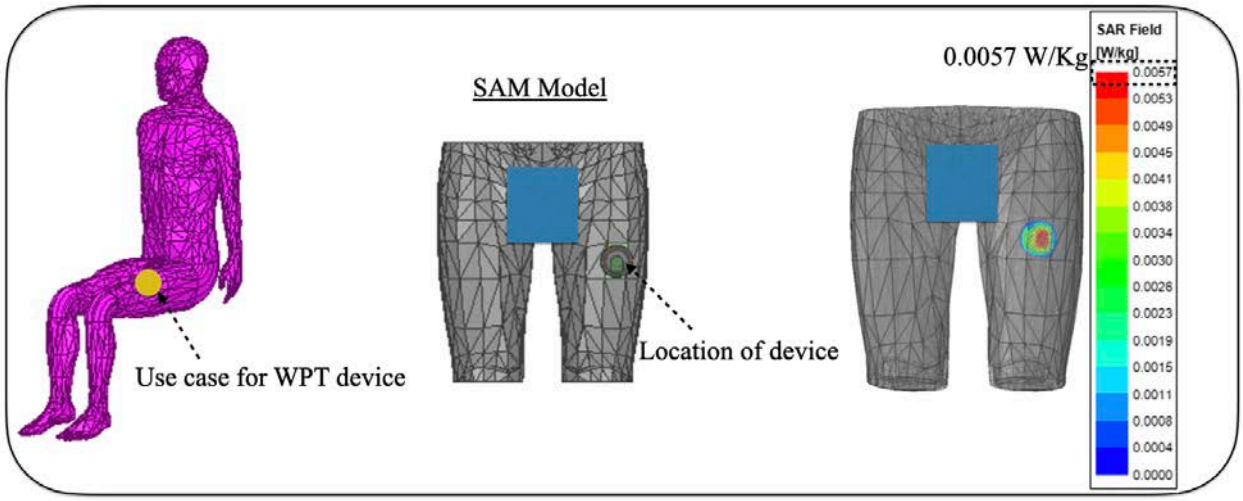

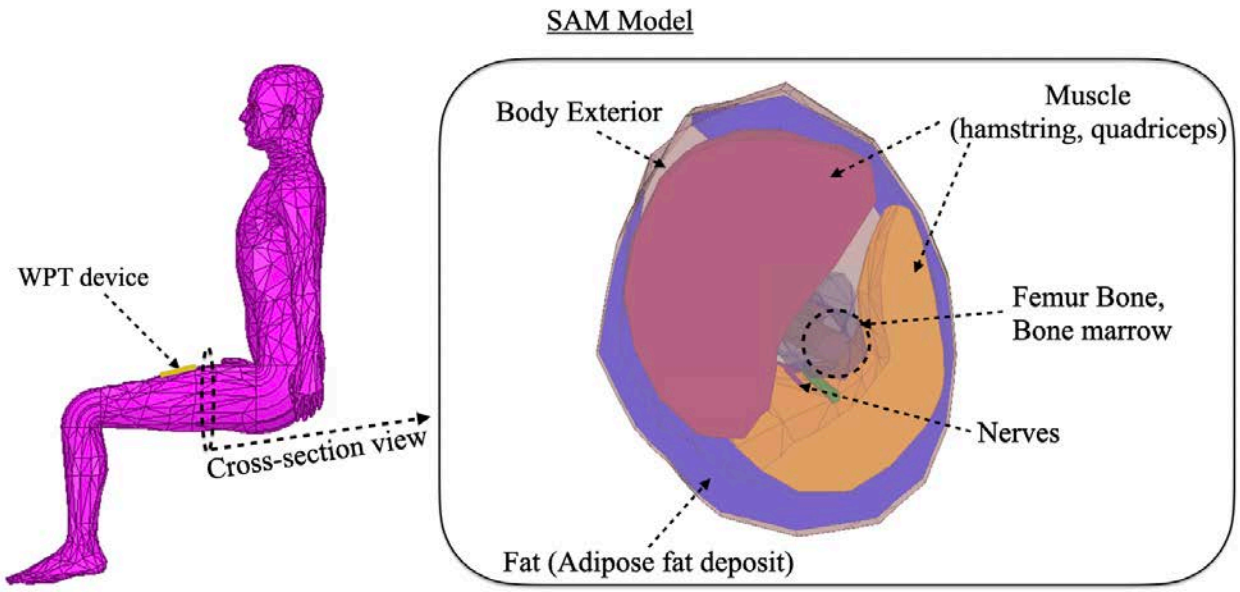
SAM Model
WPT device
Cross-section view
Body Exterior
Muscle
(hamstring, quadriceps)
Femur Bone,
Bone marrow
Nerves
Fat (Adipose fat deposit)

References:

1) **The electrical conductivity of human cerebrospinal fluid at body temperature, S.B. Baumann ; D.R. Wozny ; S.K. Kelly ; F.M. Meno, IEEE Transactions on Biomedical Engineering (Volume: 44 , Issue: 3 , March 1997)**
2) **C.Gabriel, S.Gabriel and E.Corthout: The dielectric properties of biological tissues: I. Literature survey, Phys. Med. Biol. 41 (1996), 2231-2249.**
3) **S.Gabriel, R.W.Lau and C.Gabriel: The dielectric properties of biological tissues: II. Measurements in the frequency range 10 Hz to 20 GHz, Phys. Med. Biol. 41 (1996), 2251-2269.**
4) **S.Gabriel, R.W.Lau and C.Gabriel: The dielectric properties of biological tissues: III. Parametric models for the dielectric spectrum of tissues, Phys. Med. Biol. 41 (1996), 2271-2293.**
5) **https://itis.swiss/virtual-population/tissue-properties/database/thermal-conductivity/**
6) **http://hyperphysics.phy-astr.gsu.edu/hbase/magnetic/toroid.html**
7) **X. L. Chen et al., "Human Exposure to Close-Range Resonant Wireless Power Transfer Systems as a Function of Design Parameters," in IEEE Transactions on Electromagnetic Compatibility, vol. 56, no. 5, pp. 1027-1034, Oct. 2014.**